Turkish J. Eng. Env. Sci.
32 (2008) , 323 – 335.

Determination of Susceptibility to Intergranular Corrosion of UNS 31803 Type Duplex Stainless Steel by Electrochemical Reactivation Method

Mehmet Emin ARIKAN, Mustafa DORUK
Metallurgical & Materials Engineering Department, Middle East Technical University, Ankara-TURKEY
e-mail: mdoruk@metu.edu.tr

Received 11.07.2008

Abstract

Specimens taken from a hot rolled cylindrical duplex stainless steel (DSS) bar with 22% Cr and 5% Ni grade were solution annealed at 1050 °C and then sensitization heat treatments were conducted at 650 °C. A series of specimens with ageing times ranging from 100 to 31,622 min were held for sensitization treatment. The effects of isothermal ageing treatments on the microstructure and on the localized corrosion resistance of the DSS were investigated, through the double loop electrochemical potentiodynamic reactivation (DLEPR) and standard weight loss immersion acid tests. The degree of sensitization (DOS) is measured by determining the ratio of the maximum current generated by the reactivation (reverse) scan to that of the anodic (forward) scan, $(I_r/I_a)\times 100$. The solution annealed samples and those aged at 650 °C for 100 and 316 min were found to be unsensitized, whereas samples aged 10,000 and 31,622 min were heavily sensitized. Their microstructure is composed of primary ferrite and austenite, sigma, and secondary austenite. The increased degree of sensitization can be attributed to the higher contribution of chromium and molybdenum depleted areas resulting from the formation of the intermetallic phases.

Key Words: Duplex stainless steel, Sigma phase, Secondary austenite, Electrochemical potentiostatic reactivation.

Introduction

Generally duplex stainless steels (DSSs) are Fe-Cr-Ni alloys having an approximately volumetric fraction of 50% ferrite and 50% austenite in their microstructures. Their main feature is that they comprise the favorable corrosion resistance of austenitic stainless steels with good mechanical properties (Husbands and Whitkraft, 1991).

However, DSSs are susceptible to sensitization due to the precipitation of additional phases when heated in a temperature range of 600-900 °C. All these precipitates are rich in chromium and molybdenum (Herbsleb and Schwaab, 1982). These phases affect the corrosion and mechanical properties. The sensitization temperature is often reached during isothermal heat treatment of fabricated components for stress relief, prolonged service at high temperatures, slow cooling from higher temperatures (i.e. solution annealing or during shut down of a plant operating at higher temperatures), improper heat treatment in the heat affected zone (HAZ) of the weldments, or hot working of the material (Dhooge, 1998).

Undesirable phases such as intermetallic phases (sigma and chi), carbides, and nitrides may exist in the steel if the manufacturing processes are not carefully controlled. High levels of elements stabilizing ferrite, such as chromium, molybdenum, and silicon, can promote the formation of the sigma phase

(σ). The sigma phase is a hard, brittle intermetallic phase, generally formed between 600 and 950 °C with rapid formation kinetics (Wilms et al., 1991; Kim and Kwon, 1999; Chen and Yang, 2001). Additional phases found in duplex stainless steels can include chi (χ), R, and $\alpha\prime$ (Debold, 1989). The χ phase belongs to the topologically close-packed (TCP) phases. It frequently occurs in steels, as a ternary compound containing Fe, Cr, and Mo, according to the composition $Fe_{36}Cr_{12}Mo_{10}$ (Lee et al., 1998). The nucleation sites for σ and χ phases are grain boundaries, incoherent twin boundaries, and dislocations. It is well established that the precipitation of these phases leads to a reduction in the creep ductility. It also has a reverse effect on the toughness and corrosion properties (Wilms et al., 1991). A substantial depletion of solid solution strengtheners (like Cr, Mo, C, and N), mainly due to a copious precipitation of the σ and χ phases, results in a decrease in the corrosion properties (Lopez et al., 1999).

There are several test methods for determining the sensitization to intergranular corrosion. The weight loss acid test was first standardized and the test procedure was presented in ASTM A262-02 for austenitic stainless steel. Afterwards it was standardized in ASTM A923-03 for DSS. Corrosion rate is determined by measuring the weight loss of the sample. Another test method of measuring the degree of sensitization to intergranular corrosion involves electrochemical reactivation of the steel samples as defined in ASTM G108-94. This reactivation process is named electrochemical potentiokinetic reactivation (EPR) and has been developed in single loop (SLEPR) or in double loop (DLEPR) types.

In the present study, DLEPR was applied for the determination of susceptibility to sensitization in duplex stainless steel type UNS 31803 with 22% Cr grade. It was aimed to investigate the intergranular corrosion behavior of DSS in relation to the influence of the microstructure produced by different heat treatments. Electrochemical measurements were used to determine the degree of sensitization (DOS) to intergranular corrosion. SEM and light optical microscopy (LOM) were used to identify the different phases that form in bulk material after the heat treatments. The XRD technique and EDS analysis were used for microstructural evolution. Surfaces obtained after the DLEPR test and the weight loss immersion test were also observed to check the attack locations and the relationship with the chromium depleted areas.

Experimental Method

Materials and heat treatments

The material used in this research is UNS31803 type DSS (trade name 2205 DSS). The chemical composition of the steel is given in Table 1.

Table 1. Chemical composition of 2205 DSS (wt %).

C	Cr	Ni	Mo	Mn	Fe
0.026	22.04	4.45	2.69	1.49	Ret.

The specimens were cut from a wrought cylindrical bar 100 mm in diameter and 200 mm in length. The specimens were also cylindrical and were 10 mm in diameter and 20 mm in length. They were taken from the bar in an orientation parallel to the rolling direction. In order to homogenize the structure all specimens were subjected to a solution heat treatment at 1050 °C for 1 h and then quenched in water, followed by ageing heat treatments at 650 °C for various periods of time.

Metallography

After heat treatments the surfaces of the specimens were ground with 400 to 2000 grit emery paper. For microstructure examination, the surfaces of the specimens were polished with 9 and 1 μm diamond paste. For metallographic examination, they were etched in oxalic acid (acc. ASTM A262) and NaOH solution as described in ASTM A923. The second one colors different phases in duplex stainless steel as follows: austenite in white, ferrite in light brown, sigma in dark brown, and carbides in black.

Weight loss test

The weight loss test was done according to ASTM A923-03 Test Method C standard. The test solution was prepared by dissolving 100 g of reagent grade ferric chloride ($FeCl_3.6H_2O$) in 900 ml of distilled water (6% $FeCl_3$ by weight). The pH of the solution was adjusted to approximately 1.3 by addition of HCl or NaOH. The corrosion rate was evaluated as the rate of weight loss in mg per sq. dm per day (mdd).

X-ray diffraction analysis

The metallographic examinations of specimens were done by light optical microscopy (LOM) and scanning electron microscopy (SEM). The chemical com-

position of the precipitates and the profile line analysis due to precipitation were carried out by EDS with SEM. The presence of different phases was also identified by X-ray diffraction patterns by means of Rigaku diffractometer with Cu K_α radiation.

DLEPR tests

The susceptibility of the aged DSS to intergranular corrosion was evaluated by DLEPR test, which consists of potentiokinetic scanning in a suitable electrolyte, from an active to a passive domain (activation or anodic scan), followed by a return to the initial potential (reverse or reactivation scan). The ratio of reactivation and anodic current densities permit the evaluation of the degree of sensitization (DOS).

The test was performed according to the recommendations made by Majidi and Streicher (1984). The standard solution was modified to suit DSSs and consisted of 2M H_2SO_4 + 0.5M NaCl + 0.01M KSCN at 30 ± 1 °C and a scan rate of 15 V/h. The double loop electrochemical reactivation test was done according to ASTM G108 standard.

The test was performed by running the sample from a potential lower than E_{corr} in the cathodic region. The potential is scanned in the anodic direction from E_{corr} to a point of 0.250 V in the middle of the passive region. The scanning direction is then reversed and the potential is reduced back to the cathodic region. Two loops are generated, an anodic loop and a reactivation loop. The peak activation current (I_a) and the peak reactivation current (I_r) were measured during the forward and backward scans, respectively. The degree of sensitization (DOS) was measured as the ratio of the maximum current densities generated in the double loop test (I_r/I_a)× 100 (Majidi and Streicher, 1984).

The activation or critical current density (I_a) or (I_{crit}) is proportional to the corrosion rate of a metal. The rate of corrosion rises rapidly in the activation range until the activation peak current density (I_a) is reached. The potential corresponding to this is called activation peak potential E_a or passivation potential E_{pass}. If the potential is raised further, the anodic current will drop to a lower value called passivation current density (I_{pass}), and then it will remain constant over a wide potential range. This is the passive range, in which a thin, invisible film of oxide covers the metal surface. This protective film acts as a barrier between the metal and its environment and reduces the rate of dissolution.

During the anodic sweep, the entire surface is active and contributes to the peak current. During the reactivation sweep, only the sensitized regions contribute to the passive-active transition. Thus in an unsensitized specimen there is a small I_r, and therefore a small (I_r/I_a) ratio, while in a heavily sensitized specimen I_r approaches I_a.

Results and Discussion

Metallographic examination

The optical micrographs obtained by etching with NaOH reagent are given in Figures 1 and 2. Figure 1 represents the microstructure of solution annealed parent alloy in which the white phase is austenite (γ) and the dark phase is ferrite (α). The volume fraction of α and γ was approximately 54:46. The microstructure does not reveal any visible precipitation.

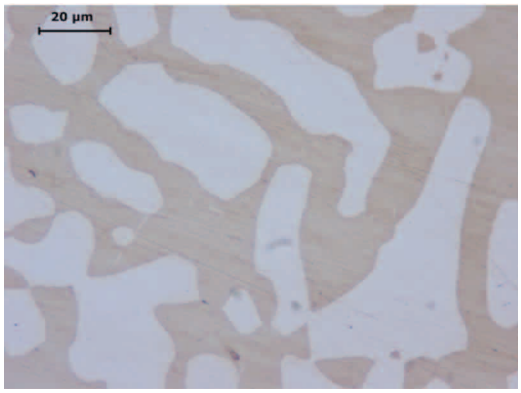

Figure 1. Microstructure of DSS, solution annealed at 1050 °C for 1 h then WQ (ferrite dark, austenite white).

To study the influence of the microstructure on DOS, the specimens were aged at 650 °C for 100, 316, 1000, 3162, 10,000 and 31,622 min. The ageing heat treatments induced a marked change in the ferrite/austenite ratio caused by the transformation (Jolly and Hochmann, 1993):

$$\alpha \rightarrow \gamma_2 + \sigma$$

where γ_2 is the so-called secondary austenite. The nucleation rate and the growth kinetics of this reaction have been studied extensively by Shek et al. (1997). It is well known that the controlling step is the nucleation rate. Growth of the sigma phase

causes a decrease in chromium and molybdenum content of the neighboring ferrite, which becomes unstable and transforms into new austenite. This austenite, in turn, is rich in chromium and molybdenum and has a lower content of nickel compared with the neighboring primary austenite. These changes in chemical composition promote the formation of an additional sigma phase. The overall result is the coprecipitation of secondary austenite and sigma.

For specimens aged at 650 °C microstructural changes are shown in Figure 2a-f. For ageing from 100 to 316 min, the first tiny precipitates appear at α/γ and α/α boundaries. Incoherent twin boundaries and dislocations inside the ferrite matrix may also be the nucleation sites for precipitation (DeBold, 1989). The precipitations of the σ phase were first encountered after ageing for 1000 min and the size

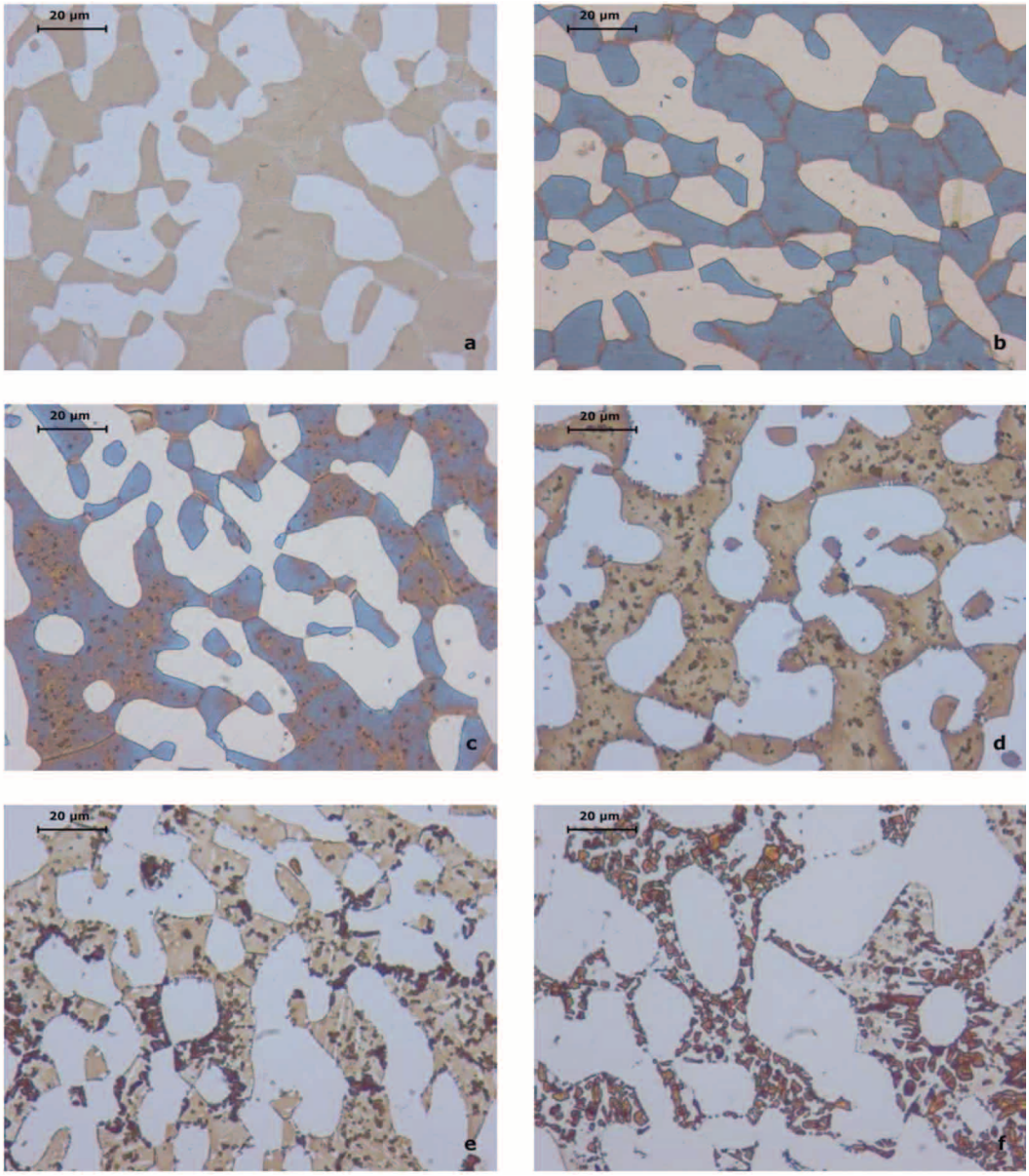

Figure 2. Optical micrographs obtained after ageing at 650 °C by etching with NaOH reagent (a) 100 min, (b) 316 min, (c) 1000 min, (d) 3162 min, (e) 10,000 min, (f) 31,622 min (austenite white, ferrite gray, sigma precipitates black).

and amount of the σ phase increased with ageing time. After 1000 min considerable sigma precipitates had developed at α/γ, α/α, and inside the ferrite phase as shown in Figure 2d-f. Longer ageing treatment leads to an increase and coarsening of the σ phase in irregular shape.

From the EDS analysis of the phases, it is seen that the σ phase is rich in chromium and molybdenum. During the growth of the sigma phase, these elements diffuse from the surrounding ferrite matrix to the sigma phase and cause depletion in these elements. The depletion in chromium and molybdenum leads to the transformation of the region to secondary austenite (γ_2).

Phase volume fraction by light optical microscopy

Microanalysis reveals that the solution annealed material consists of ferrite and austenite phases. The main microstructural change during ageing is the formation of σ-phase and secondary austenite (γ_2) from the ferrite phase due to the eutectoid reaction: $\alpha \rightarrow \sigma + \gamma_2$. The amounts of phases were estimated by measuring the fractions of colored areas on polished and etched specimens by light optical microscopy (LOM). The measured volume fractions of ferrite, austenite, and sigma phases for different ageing times and temperatures are given in Table 2. The transformation of ferrite is slow and requires a longer ageing time. The total austenite, considered the sum of the primary and secondary austenite ($\gamma + \gamma_2$), increases with time at all temperatures. The transformation is slow to reach its equilibrium value so that nearly 62% of primary ferrite remains undeformed at the end of the 31,622 min run.

Weight loss test results

The degree of sensitization is given also by the loss of weight due to the dissolution of chromium depleted areas and is expressed as the rate of weight loss in mdd. The results of the standard weight loss immersion test are given in Table 3. The corrosion rate of the specimen aged at 650 °C is low up to 1000 min and then increases rapidly up to 31,622 min. Moreover, the lower chromium and molybdenum content is not the only factor responsible for the increase in the rate of corrosion. The neighborhood of more noble phases (sigma phase) will enhance the anodic dissolution of secondary austenite extensively.

Table 2. The phase volume percentages obtained from digital image analysis.

Heat Treatment	Ageing Time (min)	Ferrite Phase %	Austenite Phase %	Sigma Phase %
Solution annealed at 1050 °C, 1 h		54.55	45.45	0
Solution annealed at 1050 °C, 1 h + Aged at 650 °C	100	54	46	0
	316	54	46	0
	1000	51.6	46.8	1.6
	3162	49.1	48.1	2.8
	10,000	44.3	49.4	6.3
	31,622	34.1	52.2	13.7

Table 3. Weight loss immersion acid test results according to ASTM A 923-03.

Ageing Time (min)	Weight Loss (mdd)
100	0.00000
316	0.01822
1000	0.50147
3162	2.42141
10,000	5.88644
31,622	7.09174

The surfaces of the corroded specimens were examined using LOM. The localized attack at black points is initiated in the secondary austenite phase adjacent to the sigma phase as shown in Figure 3. The austenite and the sigma phase resist the ferric chloride solution more compared to the ferrite and the secondary austenite. Once a pit is formed it rapidly propagates within the initial ferrite region. As a result, it is observed that the sigma and austenite phases are almost intact, while the secondary austenite (γ_2) and some iron-rich ferrite phases are attacked.

The influence of precipitates on corrosion behavior

Figure 4 shows SEM micrographs only for specimens electrolytically etched with oxalic acid after isothermal ageing at 650 °C from 100 min to 31,622 min. At ageing times shorter than 3162 min, the regions of α-ferrite were partially decomposed into σ and γ_2. At times longer than 10,000 min, the transformation showed a laminar structure of σ and γ_2 phases. The newly formed secondary austenite in the eutectoid structure seemed to be easily etched away from the surface of specimens. This is probably due to depletion of chromium and molybdenum in the γ_2 phase. As a result, in specimens aged for up to 3162 min a lot of small black pits around σ-precipitates inside ferrite regions were formed and consequently a sponge-like or porous structure developed. Sample aged for 10,000 min showed a eutectoid structure of finger-like σ and γ_2 (etched away) phases (Figure 4f). In the case of ageing for 31,622 min, the eutectoid structure of σ (coral-like structure) and γ_2 (etched away) phases was observed (Figure 4g).

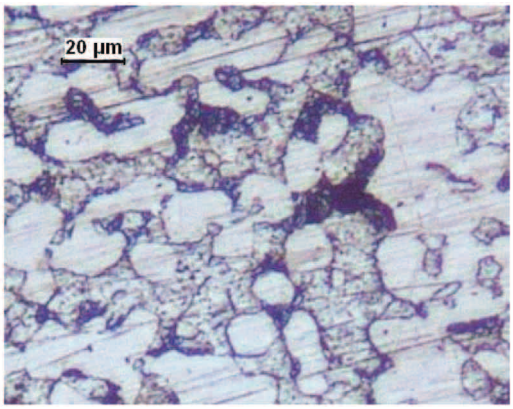

Figure 3. Dissolution of the secondary austenite in weight loss.

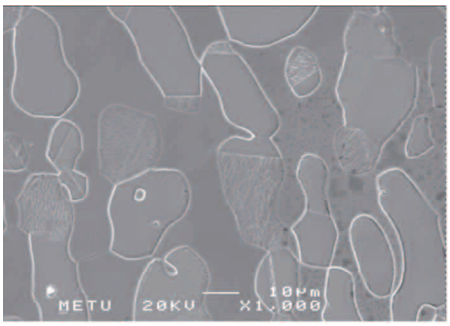

(a)

Figure 4. SEM images of specimens after electrolytic etching with oxalic acid: (a) solution annealed at 1050 °C and water quenched, then aged at 650 °C for (b) 100 min, (c) 316 min, (d) 1000 min, (e) 3162 min showing isolated sigma particles surrounded by the secondary austenite (spongy or porous structure), (f) 10,000 min showing eutectoid structure of finger-like σ and γ_2 (etched away) phases transformed from ferrite, (g) 31,622 min showing the eutectoid structure of σ (coral-like structure) and γ_2 (etched away) phases transformed from ferrite.

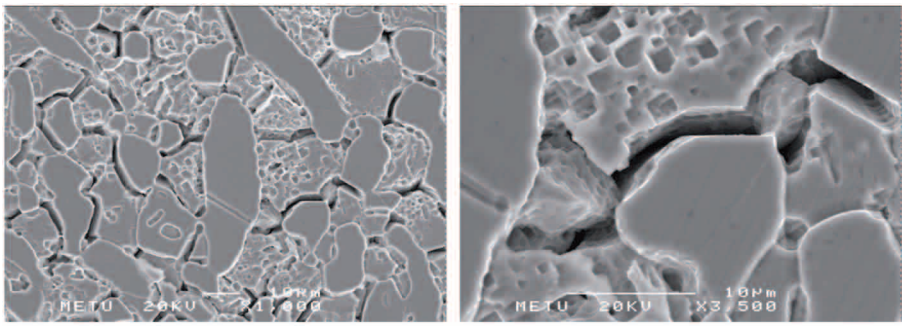

(b)

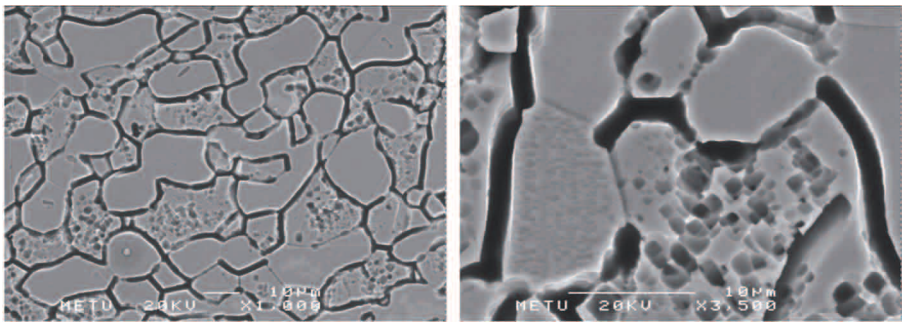

(c)

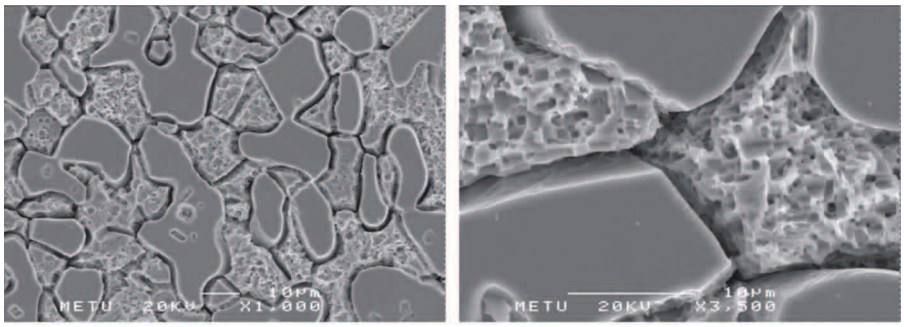

(d)

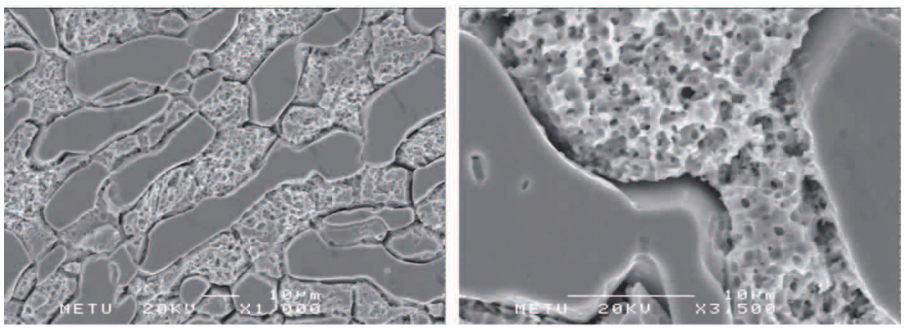

(e)

Figure 4. Continued.

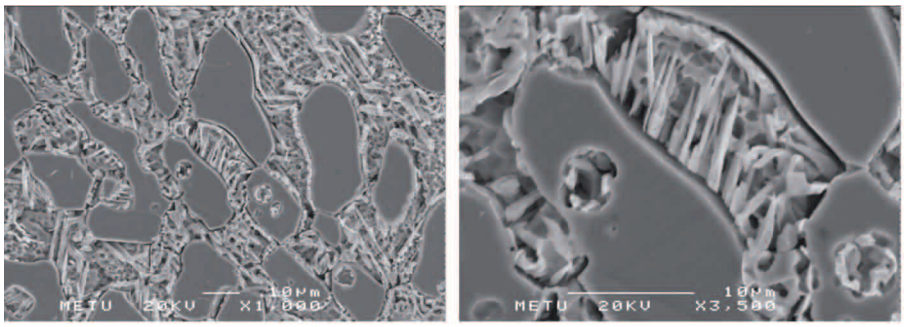

(f)

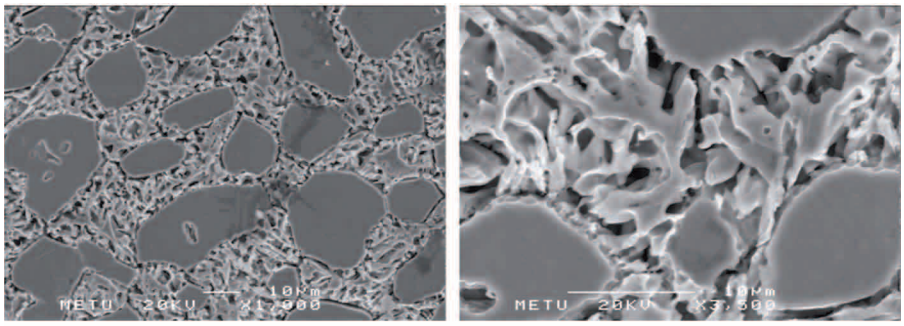

(g)

Figure 4. Continued.

EDS analysis of phases

The phases identified by EDS-SEM analysis revealed that the sigma phase appears black, the ferrite dark gray, and the primary austenite light gray (Figure 5). A bright region around the sigma phase is likely secondary austenite. The result revealed the sigma phase to be rich in chromium and the bright phase to be depleted in chromium and molybdenum with ageing time (Table 4). During the growth of the sigma phase, these elements diffuse from the surrounding ferrite matrix to the sigma phase and cause depletion in these elements. The depletion in chromium and molybdenum leads to the transformation of the region to secondary austenite (γ_2).

X-ray diffraction pattern

The results of the X-ray diffraction analysis consist of a series of diffraction patterns given in Figure 6. The diffraction pattern of the solution annealed parent alloy presents ferrite and austenite phase peaks

Table 4. EDS analysis of phases in DSS.

Heat Treatment	Phase	Cr (wt%)	Ni (wt%)	Mo (wt%)	Mn (wt%)	Si (wt%)	S (wt%)	Fe (wt%)
Solution Annealed	General composition	22.04	4.45	2.69	1.49	0.45	0.003	68.29
Solution Annealed	α	26.32	4.87	4.15	1.59	0.74	-	62.32
	γ	23.55	7.08	-	1.85	-	1.19	66.33
650 °C / 31,622 min	σ	34.68	3.32	6.13	-	-	-	55.87
	γ_2	23.82	4.62	6.44	-	0.78	-	64.34

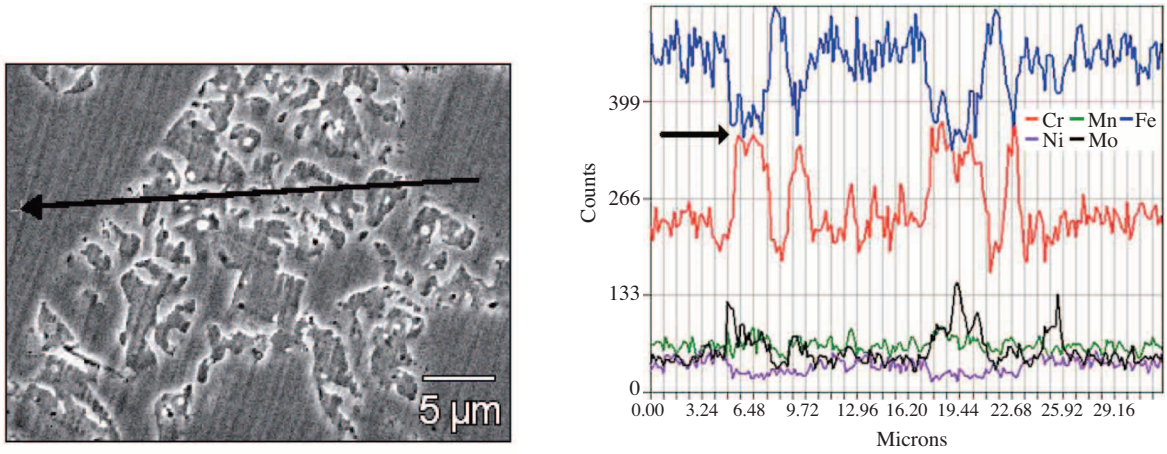

Figure 5.SEM image and profile line analysis of Cr, Ni, Mo, Mn, and Fe for the sample aged at 650 °C for 31,622 min showing chromium depleted areas due to the precipitation of σ-phase.

only. Samples aged at 650 °C do not show any peak corresponding to the sigma phase even by the end of 3162 min. This may be due to the low volume fraction of the precipitated sigma phase. The sigma phase peak first appears after 10,000 min of ageing. With increased ageing time the intensity of the sigma peak increases. After longer periods of time such as 31,622 min the treatments promote the transformation of the ferrite phase. This results in a noticeable decrease in the intensity of the α and an increase in γ peaks. The decrease in the ferrite peak intensity indicates that the major fraction of ferrite is transformed into sigma. Consequently 4 sigma peaks are observed. The changes in the diffraction peak intensity correlate well with changes in volume fraction of each phase during the isothermal hold given in Table 2.

DLEPR results

Figure 7 shows the polarization curves for samples in solution annealed and aged. The curve obtained from the solution annealed sample is treated as a reference and compared with the others. The activation current peak density (I_a) of the reference curve increased proportionally with the corrosion rate of the alloy. The anodic current peak density is 23.13 mA/cm^2 and the corresponding activation peak potential E_a, or passivation potential E_{pass} is -212.78

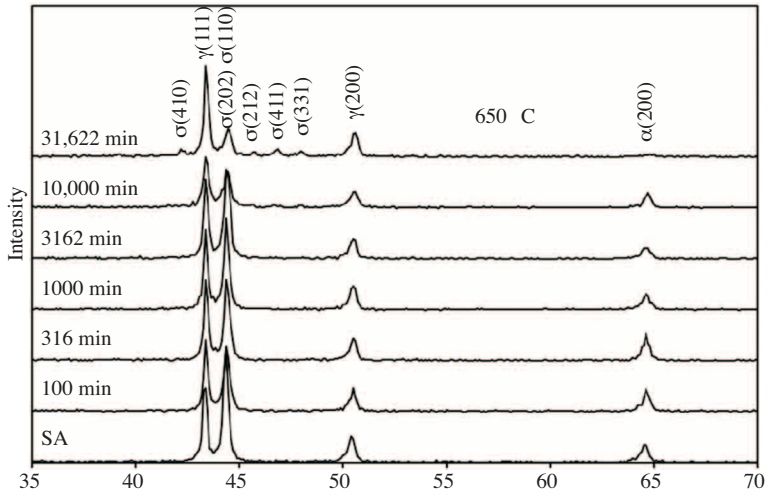

Figure 6. X-Ray diffraction patterns of samples aged at 650 °C.

mV (SCE)[1]. This peak may be attributed to the active dissolution of alloying elements. It then fell to a low passive current density (I_{pass}) of 0.001448 mA/cm^2 before reaching the chosen reverse potential of +250 mV. The sample is thus passivated in a wide range between -212.78 mV and +250 mV. In this passive range a thin, invisible film of oxide may cover the metal surface. The protective film acts as a barrier between the metal and its environment and reduces its rate of dissolution. The I_r/I_a ratio is very low (0.027634%). This may be considered unsensitized material (Table 5).

Actually, nucleation of precipitates (probably chromium carbides or nitrides and chi phase) occurs at the α/γ interface although not optically visible (Figure 2). This leads to weak chromium depletion, resulting in low sensitization because the I_r/I_a ratios are 0.033% and 0.058% for 100 and 316 min of ageing, respectively, meaning that the samples are not sensitized.

As the ageing time is increased to 1000 min fine precipitates of sigma phase first form in the ferrite phase and at α/α and α/γ boundaries (Figure 2c). The I_r/I_a ratio (3.62%) and the corrosion rate (0.50147 mdd) have increased. For an ageing time of 3162 min, the ratio is 18.57% and the corrosion rate increased to 2.42 mdd (Table 3).

In specimens aged for 10,000 and 31,622 min the precipitates reached an advanced stage of growth (Figure 2e, f). The precipitates of these sizes affect the corrosion behavior by the depletion of chromium and molybdenum in their immediate vicinity. This leads to a high I_r/I_a ratio of 49.71% and 82.42% for 10,000 and 31,622 min of ageing, respectively, showing the material to be heavily sensitized (see Table 5 for the comparison).

When the polarization curves of the samples aged at 650 °C are compared with the reference curve, it is seen that the anodic peak current densities increase with increasing ageing times (Table 5). The passive current densities increase from 0.02531 mA/cm^2 to 0.1194 mA/cm^2 and the passivation potential (E_{pass}) increases from -212.78 mV to -172.23 mV with ageing time from 100 to 31,622 min, respectively. The differences in the anodic peak current densities, passivation potentials, and the passivation current densities as compared to the reference polarization curve of the solution annealed sample can be attributed to the chromium and molybdenum depletion. This results in secondary austenite (γ_2) poorer in chromium as compared with the primary ferrite (Table 4). It originates from the primary ferrite phase because chromium diffusion is much faster in ferrite than in austenite. The chromium concentrates in the neighboring sigma phase (Wright, 2002) and causes the sigma phase to grow fast within the ferrite region. As a result, the formation of the secondary austenite can degrade the stability of the passive film (Park and Kwon, 2002).

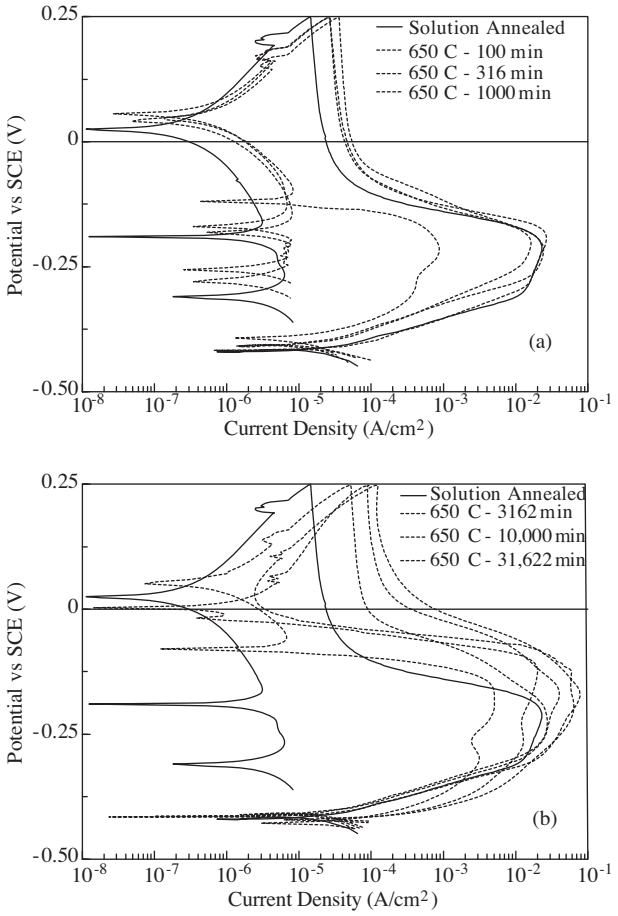

Figure 7. DLEPR curves plotted for DSS after solution and sensitization heat treatments at 650 °C between 100 and 31,622 min (scan rate: 15 V/h).

Analysis of polarization curves in reverse scanning

At the beginning of the reverse scanning, the anodic current density decreases and the anodic curve

[1] All potentials ar vs. Saturated Calomel Electrode

Table 5. DLEPR test results of 2205 type DSS.

Temperature (°C)	Time (min)	Activation Peak Potential, E_a (mV)	Activation Peak Current Density, I_a (mA/cm^2)	Reactivation Peak Potential, E_r (mV)	Reactivation Peak Current Density, I_r (mA/cm^2)	Passivation Current Density, I_{pass} (mA/cm^2)	DOS (I_r/I_a × 100)
Solution annealed at 1050 °C, 1 h		-212.78	23.1305	-267.33	0.0064	0.0014	0.0276
Solution annealed at 1050 °C, 1 h + Aged at 650 °C	100	-194.27	26.7205	-227.99	0.0089	0.0253	0.0334
	316	-201.59	16.2439	-196.26	0.0096	0.0266	0.0589
	1000	-214.66	24.1534	-218.19	0.8752	0.0338	3.6236
	3162	-229.56	27.4257	-182.82	5.0936	0.0516	18.5725
	10,000	-169.23	40.3219	-122.00	20.0460	0.0892	49.7150
	31,622	-172.23	77.7149	-194.00	64.0553	0.1194	82.4235

moves to the left (Figure 7). This is an indication of thickening of the oxide film. On decreasing the potential the anodic current density is reduced nearly to zero. This is due to the slowing of the anodic dissolution kinetics due to thickening of the passive film. The sample thus continued to passivate from E_{pass} through E_{rev} back to potential E_3. On further reduction of the potential, the direction of the current density changed between E_3 and E_4 as shown in Figure 8. It shows a loop consisting of cathodic current (Legat and Dolecek, 1995). The origin of the cathodic current can be attributed to the fact that at potentials between E_3 and E_4 the rate of the cathodic reaction is greater than the anodic current density and hence the net current is cathodic over the potential range, $\Delta E(=E_3\text{-}E_4)$ (Table 6). If the potential is further reduced on the reverse scan, the direction of the current density changes back and an anodic reactivation loop is generated. This indicates that the oxide has dissolved and a metal dissolution reaction has occurred. The development of the reactivation peak current density can be attributed to metal dissolution. The lowered reactivation peak current density I_r (on the reverse scan) is due to incomplete reactivation of the metal surface.

If no cathodic loop were generated on the reverse scan the anodic reactivation would begin at higher potential and would likely reach in a short time a high value of I_r and thus metal dissolution would take place.

The same cathodic loop behavior is observed on the reverse scans of polarization curves obtained from the solution annealed and aged samples by DLEPR test (Table 6).

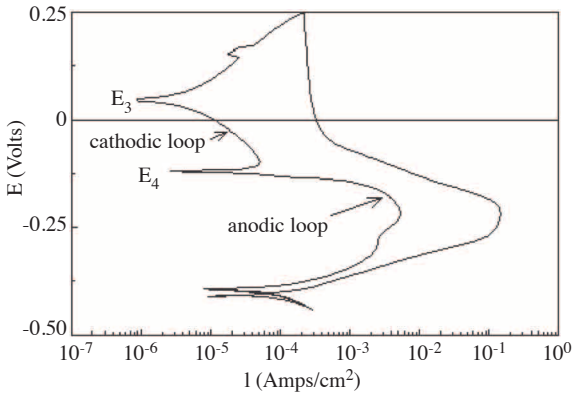

Figure 8. Cathodic and anodic loops in DLEPR curve.

Table 6. DLEPR test results on the reverse scans of polarization curves.

Temperature (°C)	Time (min)	E_3 (volt)	E_4 (volt)	ΔE (=E_3-E_4) (volt)	I_r (mA/cm^2)	DOS ($I_r/I_a \times 100$)
Solution annealed at 1050 °C, 1 h		0.0252	-0.1901	0.2153	0.0064	0.0276
Solution annealed at 1050 °C, 1 h + Aged at 650 °C	100	0.0405	-0.1808	0.2213	0.0089	0.0334
	316	0.0559	-0.1697	0.2256	0.0096	0.0589
	1000	0.0485	-0.1193	0.1677	0.8752	3.6236
	3162	0.0505	-0.0795	0.1300	5.0936	18.5725
	10,000	0.0031	-0.0178	0.0209	20.0460	49.7150
	31,622	-	-	-	64.0553	82.4235

Conclusions

The effect of isothermal treatment at 650 °C on the microstructures and consequent corrosion behavior was investigated. The important findings are summarized as follows:

- The evidence shows that the intermetallic σ-phase is first precipitated at the interface of α/γ, α/α, and inside the α-ferrite grains up to 1000 min ageing time. The σ-phase grew into coarse particles due to high diffusivity of chromium and molybdenum atoms in the ferritic structure.
- The exposure of aged samples to iron-chloride media leads to a localized and selective attack of the previous ferrite zones, partially transformed to new austenite.
- Only the solution annealed sample and those aged up to 316 min are unsensitized. However, the degree of sensitization increases rapidly with increasing ageing time.
- From the observations of the polarization curves it may also be concluded that cathodic loops do not affect metal dissolution. They merely delay the occurrence of anodic loops for a short time. The potential range ΔE (=E_3-E_4) for which the cathodic loops are obtained depends on the protective film thickness, ageing time, and thus the microstructural changes in the material.

Nomenclature

I_r	reactivation current density
I_a	activation current density
I_{pass}	passivation current density
α	ferrite phase
γ	austenite phase
σ	sigma phase
γ_2	secondary austenite
χ	chi phase
E_a	activation peak potential
E_{pass}	passivation potential

References

Chen, T.H. and Yang, J.R., "Effects of Solution Treatment and Continuous Cooling on σ-Phase Precipitation in a 2205 Duplex Stainless Steel", Mater. Sci. Eng. A Struct. Mater. Prop. Microstruct. Process, 11, 28, 2001.

Debold, T.A., "Duplex Stainless Steel-Microstructure and Properties", J. Met. March, 12-5, 1989.

Dhooge, A., "Survey on Reheat Cracking in Austenitic Stainless Steels and Ni Base Alloys", Weld World, 41, 206, 1998.

Herbsleb, G. and Schwaab, P., "Precipitation of Intermetallic Compounds, Nitrides and Carbides in AF22 Duplex Steel and Their Influence on Corrosion Behavior in Acids", P., paper presented at ASM Metals Congress, Preprint No. 8201-002, October 1982.

Husbands, J. and Whitkraft, P.K., "High-Cr Duplex Alloy in Nitric Acid Production", CORROSION/91, Paper 171, NACE, Houston, 1991.

Jolly, P. and Hochmann, J., "Structural Changes in Austenitic-Ferritic Stainless Steel on Holding Between 600 and 1150°C", Mem. Sci. Rev. Metall. 20, .117, 1973.

Kim, J.S. and Kwon, H.S., "Effects of Tungsten on Corrosion and Kinetics of Sigma Phase Formation of 25% Chromium Duplex Stainless Steels", Corrosion, 55, 512, 1999.

Lee, Y.H., Kim, K.T., Kim, K.Y. and Lee, Y.D., "Effects of W Substitution on σ and χ Phase Precipitation and Toughness in Duplex Stainless Steels", Mater. Sci. Techn., 14, 757, 1998.

Legat, A. and Dolecek, V., "Chaotic Analysis of Electrochemical Noise Measured on Stainless Steel", J. Electrochem. Soc., 142, 1851, 1995.

Lopez, N., Cid, M. and Puiggali, M., "Influence of σ-Phase on Mechanical Properties and Corrosion Resistance of Duplex Stainless Steels", Corros. Sci., 41, 1615, 1999.

Majidi, A.P. and Streicher, M.A., "The Double Loop Reactivation Method for Detecting Sensitization in AISI 304 Stainless Steels", Corrosion, 40, 584, 1984.

Park, C-J. and Kwon, H.S., "Effects of Aging at 475°C on Corrosion Properties of Tungsten-Containing Duplex Stainless Steels", Corrosion Science 44, 2817, 2002.

Shek, C.H., Wong, K.W. and Lai, J.K., "Review of Temperature Indicators and the Use of Duplex Stainless Steels for Life Assessment", Mat. Sci. Eng. R19, 5-6, 153, 1997.

Wilms, M.E., Gadgil, V.J., Krougman, J.M. and Ijsseling, F.P., "The effect of σ-Phase Precipitation at 800°C on The Corrosion Resistance in Sea-Water of a High Alloyed Duplex Stainless Steel", Corr. Sci., 36, 871, 1994.

Wright, R.N., in: R.A. Rula (Ed.), "Toughness of Ferritic Stainless Steels", ASTM STP 706, 2, 1979.